

TOWARD A DIRECT MEASUREMENT OF THE COSMIC ACCELERATION

JEREMY DARLING¹

Draft version November 21, 2012

ABSTRACT

We present precise H I 21 cm absorption line redshifts observed in multiple epochs to directly constrain the secular redshift drift \dot{z} or the cosmic acceleration, $\Delta v/\Delta t_o$. A comparison of literature analog spectra to contemporary digital spectra shows significant acceleration likely attributable to systematic instrumental errors. However, we obtain robust constraints using primarily Green Bank Telescope digital data. Ten objects spanning $z = 0.09$ – 0.69 observed over 13.5 years show $\dot{z} = (-2.3 \pm 0.8) \times 10^{-8} \text{ yr}^{-1}$ or $\Delta v/\Delta t_o = -5.5 \pm 2.2 \text{ m s}^{-1} \text{ yr}^{-1}$. The best constraint from a single object, 3C286 at $\langle z \rangle = 0.692153275(85)$, is $\dot{z} = (1.6 \pm 4.7) \times 10^{-8} \text{ yr}^{-1}$ or $\Delta v/\Delta t_o = 2.8 \pm 8.4 \text{ m s}^{-1} \text{ yr}^{-1}$. These measurements are three orders of magnitude larger than the theoretically expected acceleration at $z = 0.5$, $\dot{z} = 2 \times 10^{-11} \text{ yr}^{-1}$ or $\Delta v/\Delta t_o = 0.3 \text{ cm s}^{-1} \text{ yr}^{-1}$, but they demonstrate the lack of peculiar acceleration in absorption line systems and the long-term frequency stability of modern radio telescopes. A comparison of UV metal absorption lines to the 21 cm line improves constraints on the cosmic variation of physical constants: $\Delta(\alpha^2 g_p \mu)/\alpha^2 g_p \mu = (-1.2 \pm 1.4) \times 10^{-6}$ in the redshift range $z = 0.24$ – 2.04 . The linear evolution over the last 10.4 Gyr is $(-0.2 \pm 2.7) \times 10^{-16} \text{ yr}^{-1}$, consistent with no variation. The cosmic acceleration could be directly measured in ~ 125 years using current telescopes or in ~ 5 years using a Square Kilometer Array, but systematic effects will arise at the $1 \text{ cm s}^{-1} \text{ yr}^{-1}$ level.

Subject headings: cosmological parameters — Cosmology: observations — Cosmology: miscellaneous — dark energy — quasars: absorption lines

1. INTRODUCTION

The measurement of secular redshift drift can directly determine the cosmic acceleration² and the history of expansion in a model-independent manner (Sandage 1962; Loeb 1998) and has recently been explored in the context of dark energy and large aperture optical telescopes (e.g., Corasaniti et al. 2007; Liske et al. 2008). The magnitude of the redshift drift is minuscule, of order $5 \text{ cm s}^{-1} \text{ decade}^{-1}$ for a galaxy at redshift $z = 1$, similar to gravitational accelerations in galaxies and clusters (e.g., Amendola et al. 2008). Measuring this effect requires extreme redshift precision over time baselines of decades, and the signal may thus be overwhelmed by other systematic effects, both physical and observational. For example, secular redshift drift may be induced by proper acceleration of the observer. Such proper acceleration (but not the associated redshift drift) has been very precisely measured using pulsar timing in a Galactic reference frame (Zakamska & Tremaine 2005) and in a cosmological context using the proper motion of extragalactic radio sources (Titov et al. 2011; Xu et al. 2012). Proper acceleration of the solar system barycenter about the Galactic center creates an extragalactic dipole proper motion secular aberration drift signature on the sky that distinguishes it from a cosmological signal: objects appear to be moving toward the Galactic center. Astrometry and pulsar timing cannot, however, detect a change in the expansion rate of the universe, which is purely radial.

The observed rate of change of redshift, $\Delta z/\Delta t_o$ (hereafter \dot{z}), is the difference between a constant expansion rate at red-

shift z , $H_o(1+z)$, and its actual value $H(z)$:

$$\frac{\Delta z}{\Delta t_o} = H_o(1+z) - H(z), \quad (1)$$

where

$$H(z) = H_o \sqrt{\Omega_{M,o}(1+z)^3 + \Omega_\Lambda + (1 - \Omega_{M,o} - \Omega_\Lambda)(1+z)^2} \quad (2)$$

for a matter- and cosmological constant-dominated universe, and Δt_o is the observer's time increment (Loeb 1998). For a time-varying dark energy parameterized with scale factor-dependent equation of state $w(a) = w_o + w_a(1-a)$ (Linder 2003) where $a = 1/(1+z)$ is the scale factor, the Hubble expansion becomes

$$H(z) = H_o \sqrt{\Omega_{M,o}(1+z)^3 + \Omega_{w,o}(1+z)^{3(1+w_o+w_a)} e^{-3w_a z/(1+z)}} + (1 - \Omega_{M,o} - \Omega_{w,o})(1+z)^2. \quad (3)$$

The observed acceleration is

$$\frac{\Delta v}{\Delta t_o} = c \frac{\Delta z/\Delta t_o}{(1+z)}. \quad (4)$$

The secular redshift drift and corresponding acceleration are plotted for several cosmologies in Fig. 1; Balbi & Quercellini (2007) explore less conventional cosmological models and theories of gravity. A direct measurement of \dot{z} is completely model-independent and directly indicates the history of expansion, whatever that may be.

Here we examine the feasibility of measuring or constraining secular redshift drift using H I 21 cm absorption line systems. We demonstrate that with modern telescopes, observations spanning roughly a decade can measure redshifts to parts per 100 million and constrain the redshift drift to down a few $\text{m s}^{-1} \text{ yr}^{-1}$. Analog spectra show a systematic redshift offset from modern digital spectra, which limits the time baselines

¹ Center for Astrophysics and Space Astronomy, Department of Astrophysical and Planetary Sciences, University of Colorado, 389 UCB, Boulder, CO 80309-0389; jd darling@colorado.edu

² We use “acceleration” in the physical sense, which includes deceleration.

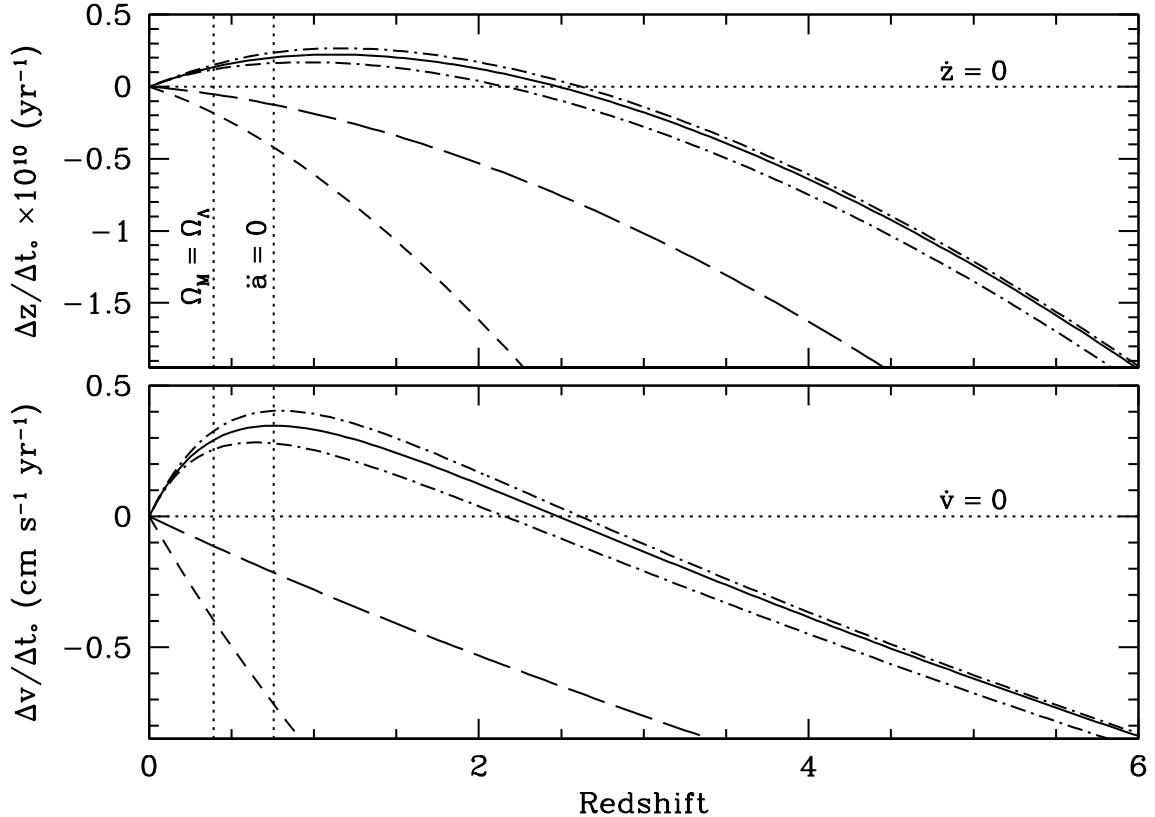


FIG. 1.— Theoretical acceleration vs. redshift. Top: Secular redshift drift (Eqn. 1). Bottom: Apparent acceleration (Eqn. 4). The solid lines show the cosmology $H_0 = 72 \text{ km s}^{-1} \text{ Mpc}^{-1}$, $\Omega_\Lambda = 0.73$, and $\Omega_M = 0.27$, the dash-dotted lines show this cosmology with a varying dark energy equation of state, $w(a) = w_0 + w_a(1-a)$ (Linder 2003), with $w_0 = -1$ and $w_a = \pm 0.5$ (lower and upper curves, respectively), the long-dashed lines show a matter-only universe with $\Omega_M = 0.27$ (open), and the short-dashed lines show a closed matter-only universe ($\Omega_M = 1.0$). Balbi & Quercellini (2007) examine \dot{z} for a panoply of less conventional models. The horizontal dotted lines indicate stationary redshift and velocity (crossing the concordance cosmology line at $z_{\dot{z}=0} = 2.48$), and the vertical dotted lines show the matter-cosmological constant equivalence redshift ($z_{M\Lambda} = 0.39$) and the transition from a decelerating to an accelerating universe ($z_{\dot{a}=0} = 0.76$).

available for \dot{z} measurements and impacts previous constraints on the cosmic evolution of physical constants that employed analog 21 cm spectra. We revise the measurement of the evolution of $\alpha^2 g_p m_e / m_p$ over the redshift span $z = 0.24$ – 2.04 .

In the following treatment of \dot{z} , we make no assumptions about cosmology; the only numbers needed are the speed of light, $c = 299792.458 \text{ km s}^{-1}$, and the rest frequency of the H I 21 cm spin-flip transition, $\nu_o(\text{HI}) = 1420.405751768 \text{ MHz}$, although neither is truly needed to measure a redshift change since it is ultimately simply a shift in the observed frequency.

2. OBSERVATIONS, DATA, AND DATA REDUCTION

Analog data provide long time baselines, in some cases more than 30 years (e.g. Wolfe et al. 1978), but we find a systematic offset toward lower redshifts compared to single-telescope digital epochs (Figure 2). These systematic offsets appear in most pre-digital spectra but are not consistent between absorption line systems, suggesting that they are instrumental and uncorrectable. We thus excluded the high quality and potentially useful observations from analog epochs. Moreover, most extant digital spectra lack the signal-to-noise needed for this study, and in order to minimize systematics we restrict all spectral epochs to those obtained using the Green Bank Telescope³ (GBT), except as noted below.

We observed 13 H I 21 cm absorption line systems in 2003–

2004 using the GBT Spectrometer and repeated the observations in 2012 (programs GBT 03C-009 and 12A-134, respectively). Five of the 13 sources include a third epoch obtained at the GBT (two) or elsewhere (three). We reduced the archival GBT Spectral Processor spectra of 0235+164 and 3C286 (program GBT 07A-021; Wolfe et al. 2011) in an identical manner to all other GBT spectra, described below. For early third epochs (ca. 2000), we used the Carilli et al. (2000) European Very Long Baseline Interferometry Network spectrum of B0218+357, the Kanekar & Chengalur (2001) Giant Metrewave Radio Telescope time-averaged spectrum of PKS 1127–145, and the Lane & Briggs (2001) Westerbork Synthesis Radio Telescope spectrum of PKS 1243–072 (all digital observations, extracted by DEXTER; Demleitner et al. (2001)). We observed 5 additional absorption line systems in single epochs (Table 1).

The two main observational epochs described here span the transition from analog to digital television. Consequently, absorption line systems that were observable through the analog radio frequency interference (RFI) comb in 2003, particularly those at $z > 1$, were no longer observable amid the digital RFI in 2012, and lines that were lost to RFI in 2003 at the upper end of the old analog television allocation, PKS1629+120 and 3C216, were detectable in 2012. These single-epoch observations are listed in Table 1 and are considered in our treatment of fundamental physical constants but are not used in the analysis of \dot{z} .

GBT observations were made in 5-minute position-

³ The National Radio Astronomy Observatory is a facility of the National Science Foundation operated under cooperative agreement by Associated Universities, Inc.

TABLE 1
REDSHIFT AND ACCELERATION MEASUREMENTS

| Absorber | z_{HI} | N_{Lines} | N_{Obs} | t_{o} (MJD) | Δt_{o} (days) | \dot{z} (yr^{-1}) | $\Delta v/\Delta t_{\text{o}}$ ($\text{m s}^{-1} \text{yr}^{-1}$) |
|---------------------|-----------------|--------------------|------------------|-------------------------|---------------------------------|-----------------------------------|--|
| 0738+313 A | 0.091234959(30) | 2 | 2 | 56041 | 3053 | $-3.0(0.9) \times 10^{-8}$ | -8.3(2.5) |
| 0738+313 B | 0.22124990(13) | 1 | 2 | 56040 | 3050 | $2.6(3.1) \times 10^{-8}$ | 6.3(7.7) |
| PKS 0952+179 | 0.2378155(16) | 1 | 1 | 52990 | ... | ... | ... |
| PKS 1413+135 | 0.24670374(30) | 2 | 2 | 55960 | 2969 | $-2.3(6.9) \times 10^{-8}$ | -5.5(16.7) |
| PKS 1127-145 | 0.312658286(20) | 4 | 3 | 55953 | 4573 | $1.4(1.0) \times 10^{-7}$ | 30.9(23.4) |
| 0248+430 | 0.39408591(14) | 5 | 2 | 55964 | 2710 | $5.8(10.6) \times 10^{-8}$ | 12.6(22.8) |
| PKS 1229-021 | 0.39498824(59) | 2 | 2 | 56137 | 2882 | $-8.4(20.8) \times 10^{-8}$ | -18.1(44.7) |
| <i>3C196</i> | 0.43667498(93) | 2 | 2 | 56136 | 2882 | $-8.0(2.5) \times 10^{-7}$ | -168(52) |
| <i>PKS 1243-072</i> | 0.4367410(14) | 1 | 3 | 56136 | 4343 | $5.8(5.1) \times 10^{-7}$ | 122(107) |
| 0235+164 | 0.523741603(72) | 4 | 3 | 55953 | 2699 | $-1.3(1.5) \times 10^{-7}$ | -25.9(28.7) |
| PKS 1629+120 | 0.5317935(11) | 2 | 1 | 56136 | ... | ... | ... |
| B3 1504+377 | 0.67324197(79) | 1 | 2 | 55968 | 2978 | $2.3(2.0) \times 10^{-7}$ | 40.6(35.3) |
| B0218+357 | 0.6846808(13) | 1 | 3 | 56038 | 4936 | $2.1(2.6) \times 10^{-7}$ | 37.1(46.2) |
| 3C286 | 0.692153275(85) | 1 | 3 | 55947 | 2956 | $1.6(4.7) \times 10^{-8}$ | 2.8(8.4) |
| <i>PKS 1830-211</i> | 0.8848633(41) | 5 | 2 | 56039 | 3048 | $-1.2(1.0) \times 10^{-6}$ | -192(163) |
| 1331+170 | 1.7763904(66) | 1 | 1 | 53105 | ... | ... | ... |
| 1157+014 | 1.943670(12) | 1 | 1 | 53070 | ... | ... | ... |
| 0458-020 | 2.0393767(21) | 2 | 1 | 53071 | ... | ... | ... |

NOTE. — For each absorption line system, z_{HI} is the error-weighted mean redshift of the strongest component in the barycentric reference frame, N_{Lines} is the number of components used to determine \dot{z} , N_{Obs} is the number of observations, t_{o} is the Modified Julian Date (MJD) of the most recent observation, Δt_{o} is the full time span of the observations, \dot{z} is the secular redshift drift, and $\Delta v/\Delta t_{\text{o}}$ is the acceleration (Eqn. 4). Parenthetical values are 1σ uncertainties. Objects in bold are those used in the \dot{z} analysis and Figure 3; those in italics are poorly constrained due to broad blended lines (3C196 and PKS 1830-211) or low signal-to-noise (PKS 1243-072). We include objects with a single digital observation for posterity, and some are compared to UV absorption lines in Figure 4.

switched (nodding) scans using two linear polarizations, 9-level sampling, 2–3 s records, a 1–1.5 s winking calibration diode injection signal, and a 12.5 MHz bandwidth centered on the H I line. Typical on-source integration times were 1–2 hours. We subtracted the corresponding off-source record from each individual on-source spectrum and normalized the difference spectrum by the sky spectrum. Each spectral record was manually examined and flagged for RFI then averaged in time and polarization. After polynomial baseline subtraction and Hanning smoothing, we typically achieved 3–24 mJy rms noise in 1.1–1.6 km s^{-1} channels at 1300–750 MHz ($z = 0.09$ –0.89) in 2003–2004, and 6–30 mJy rms noise in 0.35–0.61 km s^{-1} channels in 2012 over the same redshift range. We used GBTIDL⁴ for all GBT data reduction.

Absorption lines were fit using Gaussian profiles in each epoch and were not constrained by other epochs. Residual spectra were usually indistinguishable from line-free noise. Typically, only high signal-to-noise narrow well-separated lines were used for the \dot{z} measurement, and Table 1 lists the number of components used in each case. We measured the error-weighted mean redshift of the strongest Gaussian-fit component in each system to provide a reference redshift for posterity and to indicate the degree of precision attained (Table 1).

Figure 2 shows the spectra and time series of 0235+164, including a pre-digital epoch, as an example of the statistical uncertainties and systematic variation of the absorption lines. Weak components in the wings are only needed for good fits when the signal-to-noise is high, so these components are not included in the \dot{z} measurement. We subtract the

⁴ GBTIDL (<http://gbtidl.nrao.edu/>) is the data reduction package produced by NRAO and written in the IDL language for the reduction of GBT data.

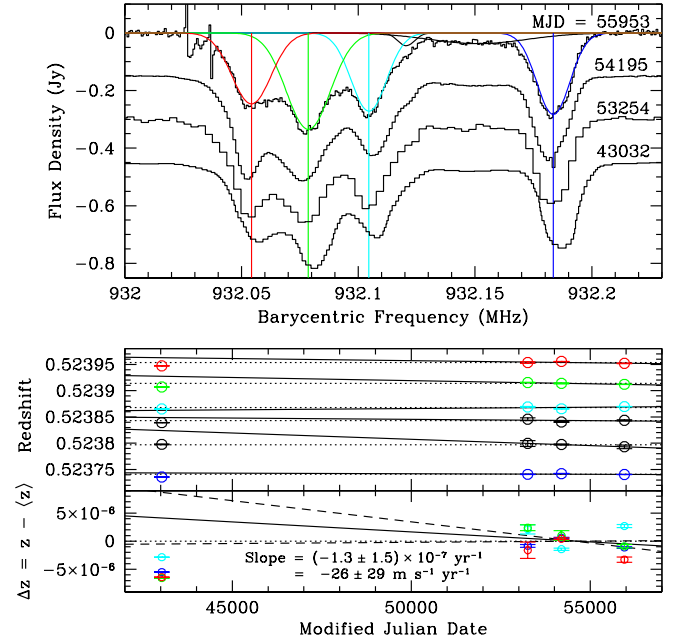


FIG. 2.— Example of redshift drift observations of an H I 21 cm absorption line system, 0235+164. Top: Spectra obtained at the GBT (upper three, all digital) and Arecibo (analog, bottom; Wolfe et al. (1978)) labeled by MJD, scaled to match the MJD 55953 blue line, and offset for clarity. Gaussian fits to well-defined lines are color-coded (others are black), matching points in the lower panel. As with many of the absorption line systems listed in Table 1, the analog spectrum of 0235+164 is systematically offset from the digital GBT spectra and is thus omitted from the linear fit. Bottom: Redshift (upper) and redshift mean offset (lower) versus MJD. Dotted lines indicate the no-drift (mean) locus in both panels, and solid lines show the linear fits, omitting the MJD 43032 analog epoch. Dashed lines show the formal error on the slope from an error-weighted linear least-squares fit.

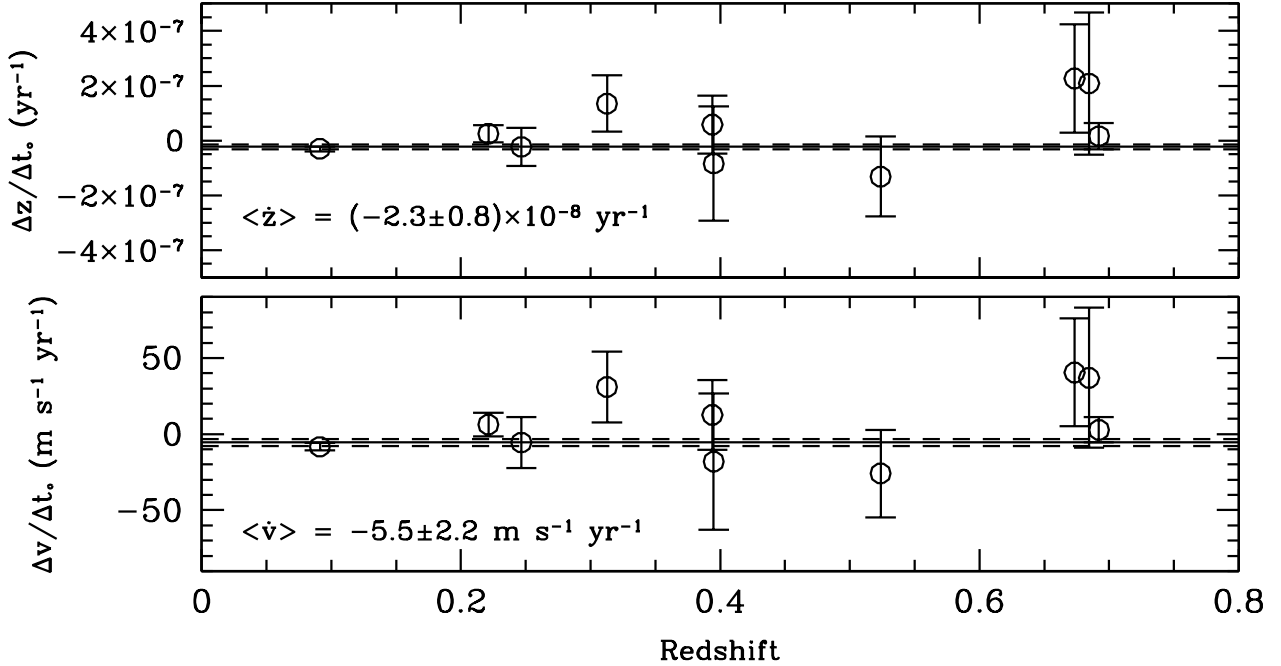


FIG. 3.— Acceleration vs. redshift of H I 21 cm absorption line systems. Horizontal lines indicate the error-weighted mean (solid) and its 1σ error (dashed). The top plot shows \dot{z} ; the bottom plot shows acceleration $\Delta v/\Delta t_0$. The error-weighted means are $\langle \dot{z} \rangle = (-2.3 \pm 0.8) \times 10^{-8} \text{ yr}^{-1}$ and $\langle \dot{v} \rangle = -5.5 \pm 2.2 \text{ m s}^{-1} \text{ yr}^{-1}$, which are dominated by 0738+313 A, 0738+313 B, PKS 1413+135, and 3C286.

error-weighted mean redshift from each component and then make an error-weighted linear fit to all reliable components simultaneously in order to average out stochastic variation among the components and obtain a bulk redshift drift of the absorber line ensemble. The slope of the linear fit is \dot{z} . We estimate the uncertainty in \dot{z} from a Monte Carlo process except for large $N_{\text{Lines}} \times N_{\text{Obs}}$ systems 0738+313 A, PKS 1127–145, 0248+430, and 0235+164, which use a formal error-weighted least-squares fitting error. The acceleration, $\Delta v/\Delta t_0$, is calculated via Equation 4 and included in Table 1.

3. RESULTS AND ANALYSIS

Figure 3 shows the secular redshift drift and acceleration of 10 absorption line systems. While the theoretical \dot{z} curves shown in Figure 1 could be fit to these data and would suggest a roughly linear trend for this redshift range, the typical measured \dot{z} value is about three orders of magnitude larger than the theoretical expectation and is consistent with zero, so we simply calculate the mean \dot{z} across redshift to assess the precision of this method and the presence (or absence) of systematic offsets from the expected value of zero.

We measure an error-weighted mean secular redshift drift of $\langle \dot{z} \rangle = (-2.3 \pm 0.8) \times 10^{-8} \text{ yr}^{-1}$ and an acceleration of $\langle \dot{v} \rangle = -5.5 \pm 2.2 \text{ m s}^{-1} \text{ yr}^{-1}$, both consistent with zero. An error-weighted linear fit fixed to $\dot{z} = 0$ at $z = 0$ has slope $-3.2 \pm 13.3 \text{ m s}^{-1} \text{ yr}^{-1}$ per unit redshift. These measurements agree with expectations and show no evidence of secular redshift drift or other systematic effects that might impair efforts to obtain higher precision, either via longer time baselines, higher signal-to-noise, or a larger sample (Sec. 4.1).

Given the systematic analog-digital offsets in H I 21 cm lines described in Sec. 2, it stands to reason that comparisons of literature analog H I lines to other absorption lines in order to measure physical constants at various redshifts are systematically affected. The redshift difference between rest-frame UV metal and H I 21 cm absorption lines measures

(or constrains) the cosmic evolution of $\alpha^2 g_p m_e/m_p$, where $\alpha = e^2/\hbar c \simeq 1/137$ is the fine structure constant, g_p is the proton gyromagnetic factor, and m_e and m_p are the electron and proton mass, respectively (Wolfe et al. 1976). Since the ratio of the H I 21 cm line to the UV metal lines scales as $\alpha^2 g_p \mu$, where $\mu = m_e/m_p$, the redshift difference between the lines can be related to fundamental constants as

$$\frac{\Delta(\alpha^2 g_p \mu)}{(\alpha^2 g_p \mu)_0} = \frac{z_{\text{UV}} - z_{21}}{1 + z_{21}} \quad (5)$$

provided the gas is velocity-coincident.

Tzanavaris et al. (2007) employed a number of analog measurements of the 21 cm lines presented in Table 1 to examine the cosmic evolution of $\alpha^2 g_p \mu$, so we revisit their analysis using digital data. Figure 4 shows the normalized redshift difference between H I 21 cm lines and UV metal lines for the nine absorption line systems measured by Tzanavaris et al. (2007) and for the seven systems measured by us using the GBT. The UV line ensemble redshifts are presented in Tzanavaris et al. (2007). In two cases we use a 21 cm component that is not the dominant one for comparison to the UV lines: in 0235+164 we use the H I line at $z = 0.52384114(41)$, the strongest of the line triplet (Fig. 2), to match the component used by Tzanavaris et al. (2007), and in 0458–020 we use the redder component at $z = 2.0395474(64)$ that matches the many UV lines presented in Tzanavaris et al. (2007).

Despite the smaller sample, we obtain a substantially reduced error-weighted mean: the fractional change in $\alpha^2 g_p \mu$ is $(-1.2 \pm 1.4) \times 10^{-6}$ in the redshift range $z = 0.24$ – 2.04 . An identical treatment of the Tzanavaris et al. (2007) data yields a fractional change of $(+19.9 \pm 3.0) \times 10^{-6}$ (using their statistical error bars for consistency). The unweighted means are similar, $(+2.9 \pm 5.5) \times 10^{-6}$ (this work) versus $(+5.3 \pm 9.9) \times 10^{-6}$ (Tzanavaris et al. 2007), and our uncertainty is roughly half despite the slightly smaller sample.

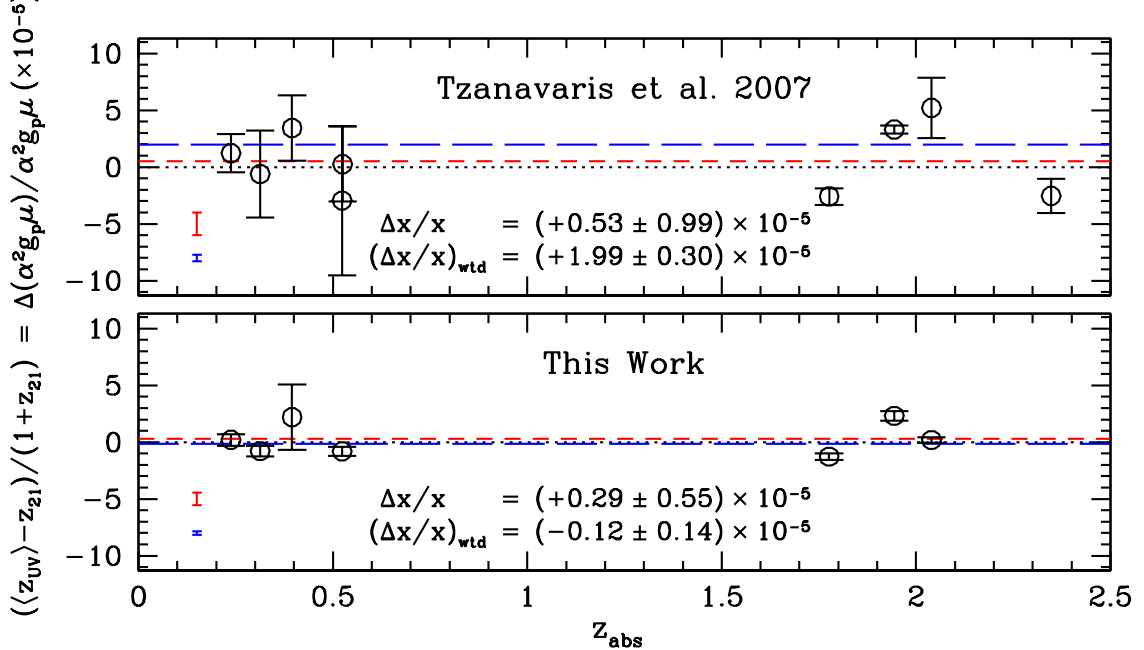


FIG. 4.— The fractional redshift difference between UV metal and 21 cm H I absorption lines vs. redshift. This is equivalent to the fractional change in $\alpha^2 g_p \mu$. Top: Reproduction of the Tzanavaris et al. (2007) plot using literature 21 cm absorption lines and their statistical error bars. Bottom: the same plot using GBT-measured H I 21 cm lines. Horizontal lines indicate the null line (dotted), the mean (red, short dashed), and the error-weighted mean (blue, long-dashed). Error bars in the lower left of each panel indicate the uncertainties in each mean value. Despite the smaller sample, our mean offsets are significantly smaller and their uncertainties are smaller by a factor of two. Individual error bars are likewise substantially smaller due to higher signal-to-noise in most 21 cm observations.

The linear evolution over the last 10.2 Gyr⁵, assuming the laboratory value at $z = 0$, is $(-0.2 \pm 2.7) \times 10^{-16} \text{ yr}^{-1}$, consistent with no variation. A negative value indicates a positive slope in Fig. 4 (the value decreases as time advances from the early universe to the present). Tzanavaris et al. (2007) obtained a limit one order of magnitude larger, $(-0.6 \pm 1.2) \times 10^{-15} \text{ yr}^{-1}$, using their favored analysis.

4. DISCUSSION

4.1. \dot{z}

The intrinsic stability of the H I 21 cm lines does not seem to be an issue at the level of a few $\text{m s}^{-1} \text{ yr}^{-1}$. Most systems show negligible epoch-to-epoch redshift variation, but a few systems such as PKS 1127–245 do show significant apparently stochastic variation, and the measured \dot{z} may be affected by the time of measurement and the number of epochs. Stochastic line shifts of order 500 m s^{-1} over time scales of about 1 year with no net change in the mean line velocity have been observed (Wolfe et al. 1982; Briggs 1983) as well as variation in line depth (e.g., Kanekar & Chengalur 2001), and the common interpretation is that a variable illuminating radio source structure picks out varying portions of the foreground absorbing clouds. This effect may become significant as one approaches the precision needed to detect the expected cosmological acceleration.

Gravitational accelerations of order $1 \text{ cm s}^{-1} \text{ yr}^{-1}$ are likely in galactic and extragalactic settings, such as the acceleration of galaxies in clusters and the orbital accelerations within galaxies (Amendola et al. 2008). For example, the Solar System barycenter accelerates toward the Galactic Center at $\sim 0.7 \text{ cm s}^{-1} \text{ yr}^{-1}$, assuming a circular orbit. Extragalactic gravitational accelerations are distinguishable from the cosmic \dot{z}

because they will be randomly distributed, showing both positive and negative values, and will not be coherent across the sky or depend on redshift. The barycenter acceleration will appear in \dot{z} measurements as a redshift-independent acceleration dipole on the sky.

Our \dot{z} measurement depends primarily on the four best-measured absorption line systems; omitting points with error bars greater than $20 \text{ m s}^{-1} \text{ yr}^{-1}$ has a negligible impact on the result, which suggests that only ~ 10 additional systems with uncertainties of order a few $\text{m s}^{-1} \text{ yr}^{-1}$ would improve this measurement substantially, perhaps below $1 \text{ m s}^{-1} \text{ yr}^{-1}$.

To estimate the time required to measure the canonical cosmological \dot{z} at $z = 1$ ($\dot{z} = 2 \times 10^{-11} \text{ yr}^{-1}$), we assume a scenario whereby an ensemble of 30 lines is observed once per year with uncertainty $\sigma_{\dot{z}} = 5 \times 10^{-8}$ per line per observation. We claim a detection when the uncertainty of a linear fit of redshift versus time recovers the slope with at least 3σ significance. For the GBT, a direct detection of \dot{z} will require about 300 years. For a Square Kilometer Array (SKA) with ~ 130 times the collecting area, $\sigma_{\dot{z}} \simeq 4 \times 10^{-10}$ and this measurement can be made in about 12 years, which is competitive with a 42 m optical telescope observing Lyman α forest lines over ~ 20 yr (Liske et al. 2008). If the number of lines increases to 300, an expected dividend of upcoming SKA prototype surveys such as those planned for ASKAP (Johnston et al. 2008; Darling et al. 2011), then the GBT measurement would require ~ 125 years, and the SKA measurement ~ 5 years.

4.2. Physical Constants

H I 21 cm lines are no longer the limiting factor in constraining the cosmic evolution of $\alpha^2 g_p \mu$: UV metal line redshift uncertainties are 1–2 dex larger than the 21 cm line uncertainties at $z < 1$ and are comparable at $z > 1$. Systematic effects, such as the coincidence of the 21 cm- and UV line-producing regions do not yet appear to be significant. Sys-

⁵ From present to $z = 2.04$, assuming $H_0 = 72 \text{ km s}^{-1} \text{ Mpc}^{-1}$, $\Omega_\Lambda = 0.73$, and $\Omega_M = 0.27$.

tematic offsets between analog and digital 21 cm redshifts suggest that other astronomical tests of the cosmic variation of physical constants employing analog 21 cm data should be re-examined.

Recent studies using modern radio line observations are consistent with no evolution in $\alpha^2 g_p \mu$, albeit with larger uncertainties than our result: Wolfe et al. (2011) obtain a 2σ limit $\Delta(\alpha^2 g_p \mu)/\alpha^2 g_p \mu < 6 \times 10^{-6}$ using 3C286 alone, based on the identification of the observed optical absorption with a specific H I-absorbing cloud, and Kanekar et al. (2010) compared 21 cm to UV C I absorption in two systems at $z \sim 1.5$ to find $(6.8 \pm 1.0_{\text{stat}} \pm 6.7_{\text{sys}}) \times 10^{-6}$. Recent UV-H I comparisons obtaining similar-uncertainty measurements to ours include Rahmani et al. (2012) with $(-0.1 \pm 1.3) \times 10^{-6}$ at $\langle z \rangle = 1.36$ and Srianand et al. (2010) who find $(-1.7 \pm 1.7) \times 10^{-6}$ in a single absorber at $z = 3.17$.

5. CONCLUSIONS

We have obtained a precise constraint on the cosmic acceleration by directly measuring the real-time secular redshift drift of H I 21 cm absorption line systems. We measure a redshift drift of $\langle \dot{z} \rangle = (-2.3 \pm 0.8) \times 10^{-8} \text{ yr}^{-1}$ and an acceleration

$\langle \ddot{v} \rangle = -5.5 \pm 2.2 \text{ m s}^{-1} \text{ yr}^{-1}$, both consistent with no acceleration. These measurements have not yet reached the theoretically expected acceleration, $\dot{z} = 2 \times 10^{-11} \text{ yr}^{-1}$ or $\Delta v/\Delta t_0 = 0.3 \text{ cm s}^{-1} \text{ yr}^{-1}$ at $z = 0.5$, but they demonstrate an encouraging lack of peculiar acceleration in absorption line systems and the frequency stability of modern radio telescopes required for repeatable measurements. We thus find no significant systematic effects that would impede even more precise measurements, which may be done by expanding the sample, using longer time baselines, larger redshifts, and higher signal-to-noise observations, particularly from larger apertures. Systematic effects will be significant below $1 \text{ cm s}^{-1} \text{ yr}^{-1}$, but direct measurements of the cosmic acceleration using multiple methods, wavelengths, and telescopes will likely be possible in a few decades.

We thank the GBT and NRAO staff for supporting this project and for building and operating an exquisitely sensitive and stable telescope. We also thank the referee for helpful comments. This research made use of the NASA/IPAC Extragalactic Database (NED) which is operated by the Jet Propulsion Laboratory, California Institute of Technology, under contract with NASA.

REFERENCES

Amendola, L., Balbi, A., & Quercellini, C. 2008, Physics Letters B, 660, 81
 Balbi, A. & Quercellini, C. 2007, MNRAS, 382, 1623
 Briggs, F. H. 1983, ApJ, 274, 86
 Carilli, C. L., Menten, K. M., Stocke, J. T., Perlman, E., Vermeulen, R., Briggs, F., de Bruyn, A. G., Conway, J., & Moore, C. P. 2000, Phys. Rev. Lett., 85, 5511
 Corasaniti, P.-S., Huterer, D., & Melchiorri, A. 2007, Phys Rev D, 75, 062001
 Darling, J., Macdonald, E. P., Haynes, M. P., & Giovanelli, R. 2011, ApJ, 742, 60
 Demleitner, M., Accomazzi, A., Eichhorn, G., Grant, C. S., Kurtz, M. J., & Murray, S. S. 2001, ASP Conf. Proc., Astronomical Data Analysis Software and Systems X, eds. F. R. Harnden, Jr., F. A. Primini, H. E. Payne, 238, 321
 Johnston, S., Taylor, R., Bailes, M., et al. 2008, Experimental Astronomy, 22, 151
 Kanekar, N. & Chengalur, J. N. 2001, MNRAS, 325, 631
 Kanekar, N., Prochaska, J. X., Ellison, S. L., & Chengalur, J. N. 2010, ApJ, 712, L148
 Lane, W. M. & Briggs, F. H. 2001, ApJ, 561, L27
 Linder, E. V. 2003, Phys. Rev. Lett., 90, 091301
 Liske, J., Grazian, A., Vanzella, E., et al. 2008, MNRAS, 386, 1192
 Loeb, A. 1998, ApJ, 499, L111
 Rahmani, H., Srianand, R., Gupta, N., Petitjean, P., Noterdaeme, P., & Vásquez, D. A. 2012, MNRAS, 425, 556
 Sandage, A. 1962, ApJ, 136, 319
 Srianand, R., Gupta, N., Petitjean, P., Noterdaeme, P., & Ledoux, C. 2010, MNRAS, 405, 1888
 Titov, O., Lambert, S. B., & Gontier, A.-M. 2011, A&A, 529, A91
 Tzanavaris, P., Murphy, M. T., Webb, J. K., Flambaum, V. V., & Curran, S. J. 2007, MNRAS, 374, 634
 Webb, J. K., King, J. A., Murphy, M. T., Flambaum, V. V., Carswell, R. F., & Bainbridge, M. B. 2011, Phys. Rev. Lett., 107, 191101
 Wolfe, A. M., Brown, R. L., & Roberts, M. S. 1976, Phys. Rev. Lett., 37, 179
 Wolfe, A. M., Broderick, J. J., Johnston, K. J., & Condon, J. J. 1978, ApJ, 222, 752
 Wolfe, A. M., Davis, M. M., & Briggs, F. H. 1982, ApJ, 259, 495
 Wolfe, A. M., Jorgenson, R. A., Robishaw, T., Heiles, C., & Prochaska, J. X. 2011, ApJ, 733, 24
 Xu, M. H., Wang, G. L., & Zhao, M. 2012, A&A, 544, A135
 Zakamska, N. L. & Tremaine, S. 2005, AJ, 130, 1939